CONSTRUCTION OF THE TWO FOOT CLOUD CHAMBER

AND

SOME PRELIMINARY RESULTS ON COSMIC RAY ENERGY DISTRIBUTION

AT SEA LEVEL

A Thesis

Submitted in Partial Fulfillment

of the Requirements for the degree of

Doctor of Philosophy

at

The California Institute of Technology

Pasadena, California.

by

LEON KATZ

1943

This thesis is in the nature of a progress report on the large two foot cloud chamber being built by Dr. Carl D. Anderson and Dr. Seth Nadermeyer. The thesis will serve the double purpose of recording and making available the experience of the cosmic ray gro up in building the chamber as well as reporting the results of some preliminary measurements.

CONSTRUCTION

The general layout of the chamber, magnetic poles, cameras and lights is shown in Fig. 1. The optical system is shown in greater detail in Fig. 2. See also photograph of Fig. 10. The mirror and cameras are mounted as a unit which may be easily removed from the cloud chamber and used for reprojecting the tracks. The advantages of this set-up are obvious, since, with the sole exception of the plate glass forming the front of the chamber the same optical system that is used in photographing is used in reprojecting the film. Thus distortions from this source are automatically eliminated. To approximate the actual optical system even more closely the tracks are projected through a sheet of plate glass similar to that which forms the front of the cloud chamber, placed at approximately the same position in the optical path.

A cross section of the cloud chamber proper is shown in Fig. 3. The diaphragm, whose design was arrived at through a process of evolution, seems to operate satisfactorily. A few of the difficulties met with in alternative designs are as follows: a simple rubber diaphragm coming to rest against a perforated plate acting as a stop, seems to generate a high

GENERAL ASSEMBLY OF CLOUD CHAMBER, MAGNET, LIGHTS
and
CAMERAS.

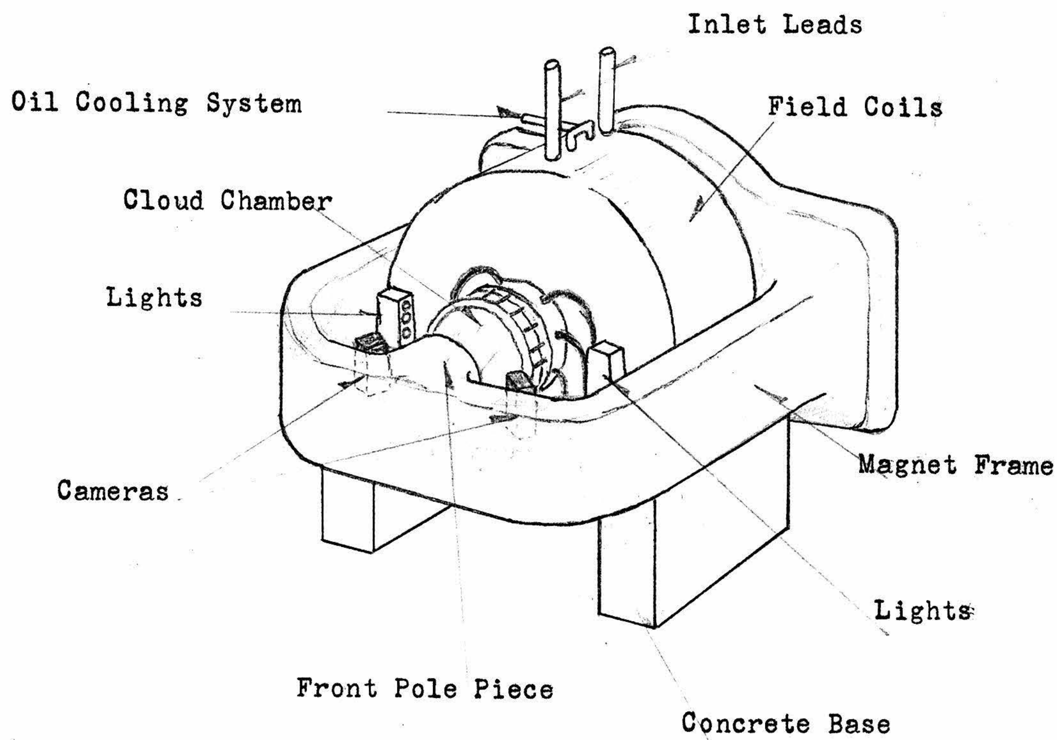

Fig.1

Leon Katz 1-25-43

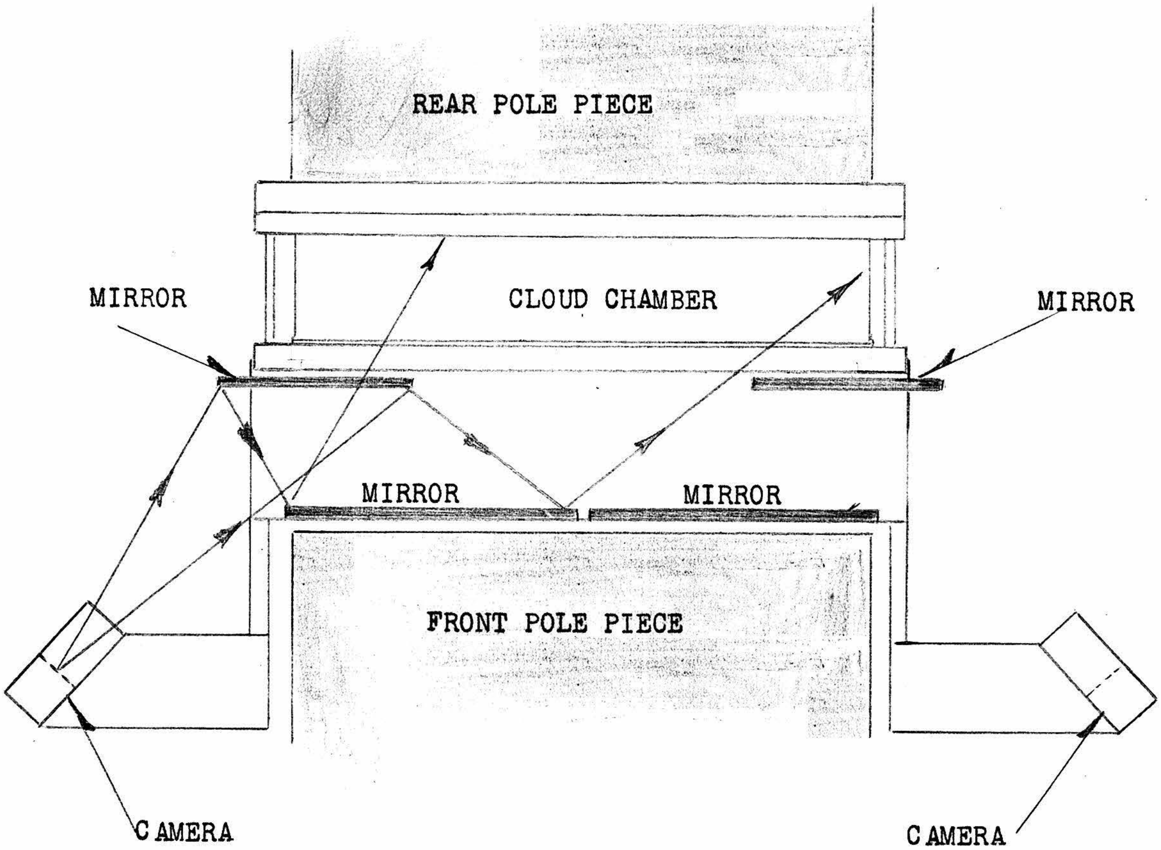

Figure 2.

Lyon, Katz 1-25-43

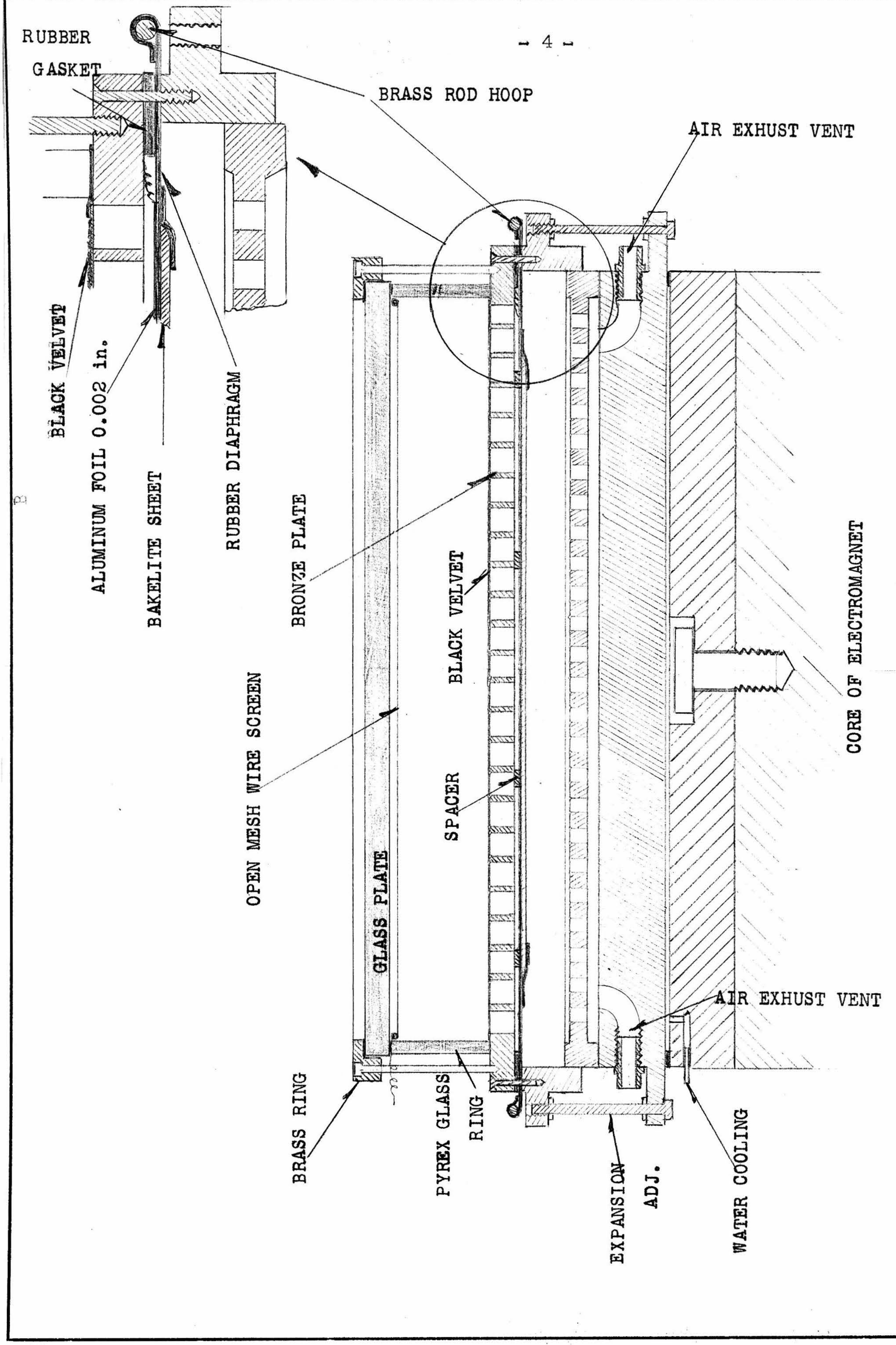
RUBBER GASKET
BRASS ROD HOOP
AIR EXHUST VENT
BLACK VELVET
ALUMINUM FOIL 0.002 in.
BAKELITE SHEET
RUBBER DIAPHRAGM
BRONZE PLATE
BLACK VELVET
OPEN MESH WIRE SCREEN
SPACER
GLASS PLATE
CORE OF ELECTROMAGNET
AIR EXHUST VENT
BRASS RING
PYREX GLASS RING
EXPANSION ADJ.
WATER COOLING

Figure 3.

electrostatic potential when it pulls away rapidly as the chamber expands, and gives rise to ions which contaminate the chamber; on the other hand if the rubber has a bakelite sheet glued to it for stiffness and the motion of the system is limited by a number of pegs placed around the perifery, then even a slight excess of pressure behind the diaphragm will buckle it sufficiently to cause distortion of the tracks due to the uneven mass motion of the air on expansion.

The construction of the diaphragm as finally used will now be described. The first step in the construction was to stretch a sheet of rubber $\frac{1}{32}$ inch thick on a brass hoop, Fig. 3. Then a $\frac{3}{16}$ inch circular sheet of bakelite $22\frac{1}{4}$ inches in diameter, whose edges were thinned down, was fastened to the rubber with bakelite cement (see below). The edges of the bakelite sheet were then secured with a strip of rubber; half of the rubber strip on the bakelite sheet was glued with bakelite cement, the other half was fastened by rubber cement to the rubber.

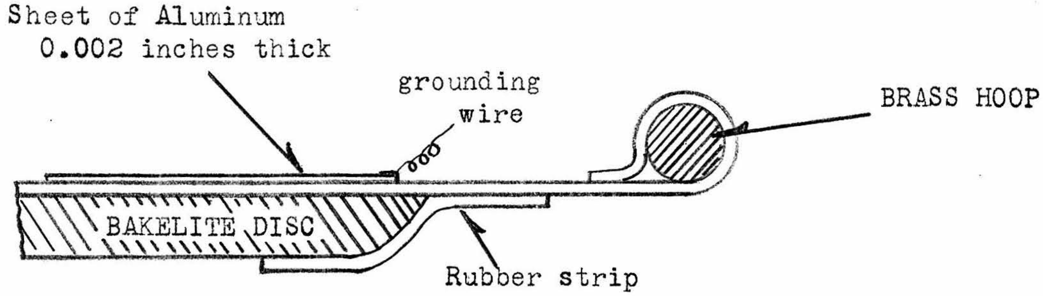

A sheet of aluminum foil 0.002 inches thick was then glued with bakelite cement to the rubber sheet on the opposite side of the bakelite disc. It was found convenient to iron the foil down with a warm pressing iron, which smoothed it out and fastened it more securely. Thin flexible grounding wires were then fastened to the aluminum on one end and grounded to the cloud chamber on the other. The end fastened to the foil was secured with a copper sheet clip as shown:

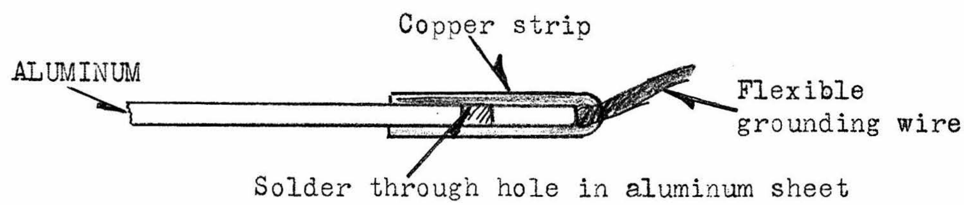

As will be seen from Fig. 3. the diaphragm in the compressed position does not rest directly against the perforated bronze plate, but is held away from it by a number of small stops, these are for the purpose of avoiding local overexpansions. Care was taken to avoid any such 'dead' spaces which might cause local over-expansions and thus contaminate the chamber.

When compressing the chamber, the air pressure behind the diaphragm is slowly raised until the diaphragm rests securely against these stops. Graph 1 shows the chamber pressure as a

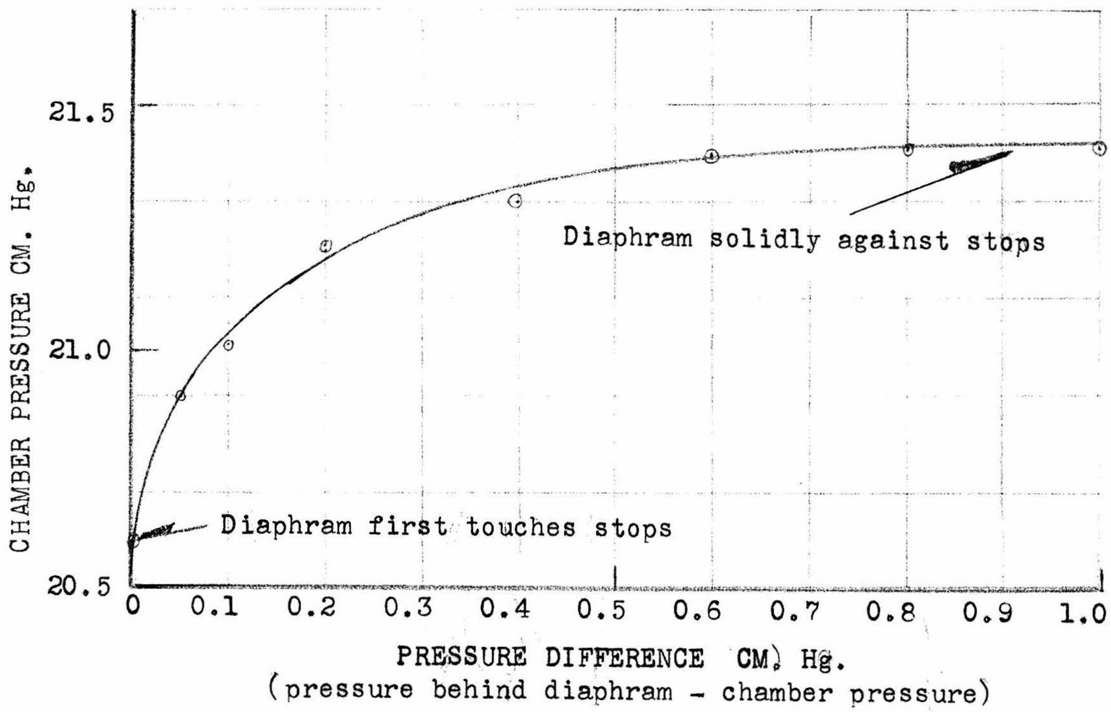

Graph 1

L. Katz

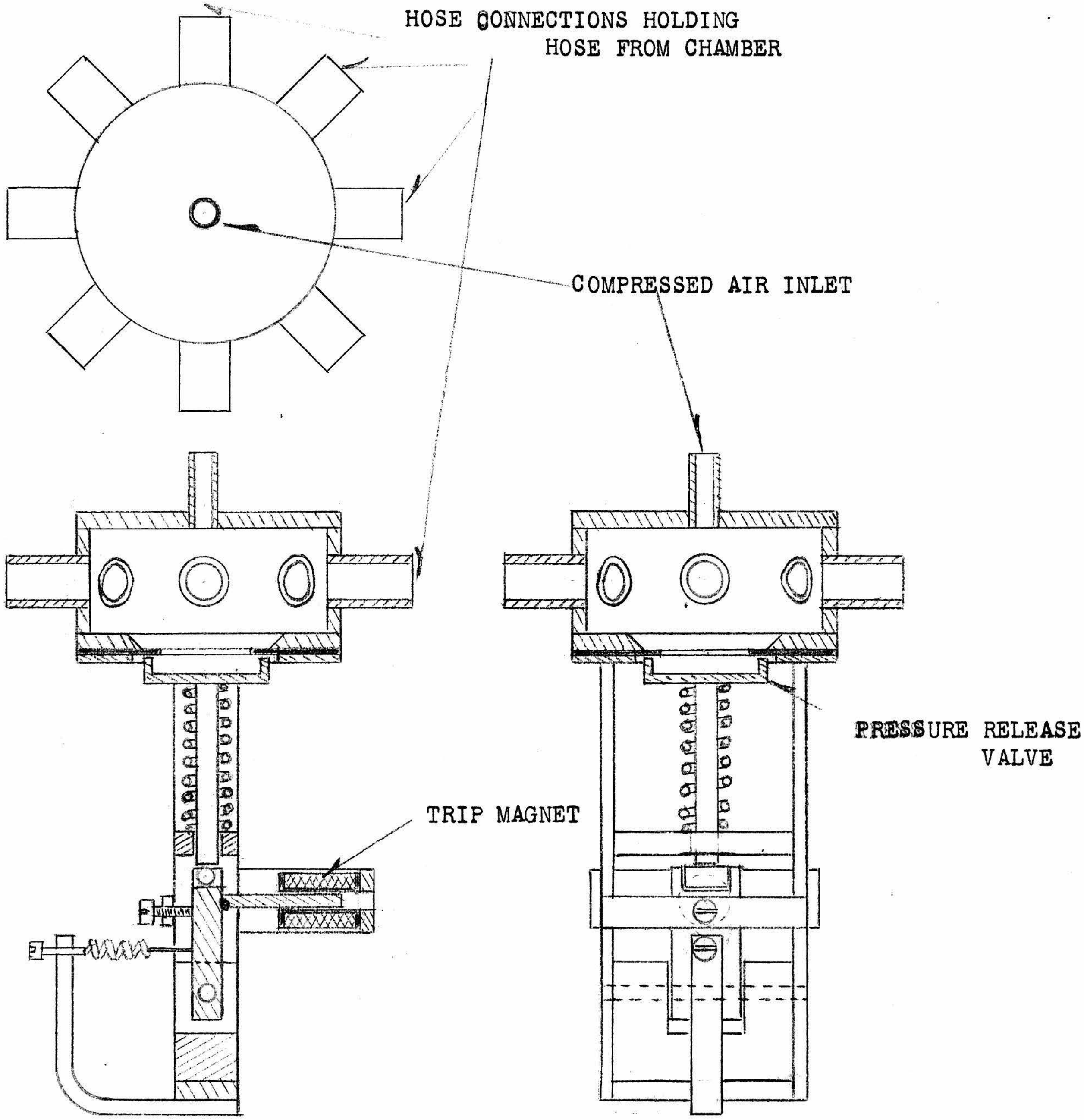

EXPANSION VALVE

Fig.4

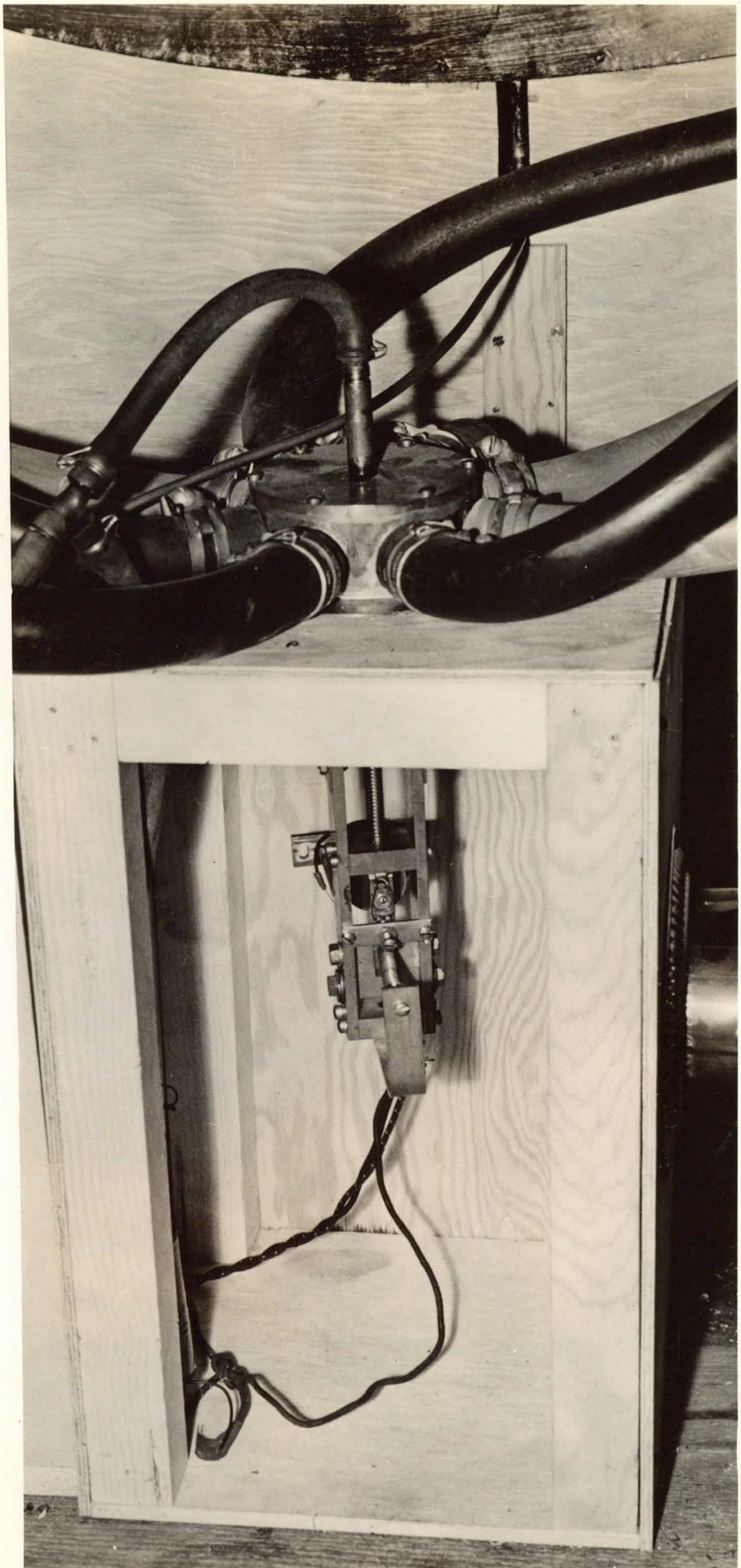

Fig. 4b

function of the pressure difference across the diaphragm. It will be seen that about 0.6 cm. of Hg pressure is sufficient to bring the diaphragm to its limit of motion in the forward direction.

The ratio of expansion is limited by the distance which the diaphragm is allowed to travel in its backward motion. This distance is adjusted by moving the chamber closer or further from the back pole of the magnet by three screws. The rapid expulsion of the air from behind the diaphragm is achieved by the use of eight two inch hose symmetrically connected with the chamber and linking it with the expansion valve, which is of a conventional design as sketched in Fig. 4, and shown in photograph Fig. 4b.

With this arrangement, the width of tracks due to the diffusion of ions indicates that about 0.02 seconds elapse between the instant the counters are tripped and when expansion is completed (ions weighted down with water drops.)

The problem of illuminating a chamber with sufficient light intensity to photograph the minute droplets of water has always been a difficult one. In this case it was resolved by the use of two argon filled stroboscopic lamps. These, when placed in an optical system to be described, and each fired by a 48μf condenser at 5000 volts, give sufficient light to register the tracks on XX-super pan film at an f8 lens opening.

It was necessary to construct the lamps from quarts tubing to withstand the high temperature developed in them when flashed. See Fig. 5. They were filled to about 30 cm. of Hg. pressure with argon (of commercial purity 99.6%) after being thoroughly outgassed. Tests indicate that the intensity of illumination from the flash is not sensitive to pressure changes of a few centimeters of Hg. of the gas within the lamps.

Each lamp was enclosed in a wooden box, one side of which had three $4\frac{1}{2}$ inch focal length plano-convex lenses (type used in condensers) as shown in Fig. 5. The beam of light obtained by the use of these lenses was limited to a fairly well defined sheet about $1\frac{1}{2}$ inches wide and 30 inches high.

The lamps were flashed by a controlling circuit shown in Fig. 6. The circuit which expands the chamber (to be described later) impresses a pulse on the input of the time delay circuit, where the signal is delayed an appropriate time to allow the drops of moisture to grow on the ions forming the cosmic ray track (about $\frac{1}{20}$ sec.). The delay

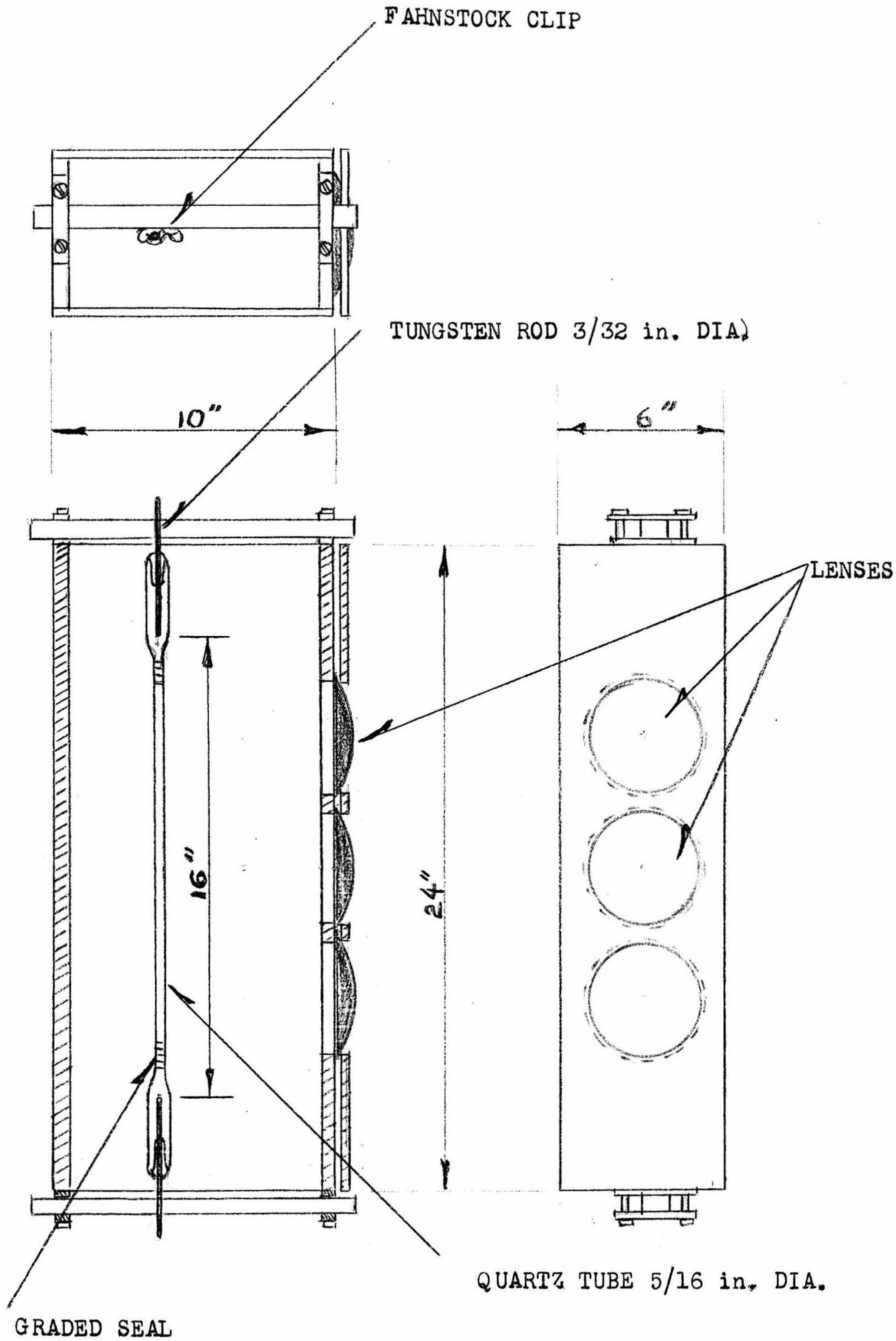
FAHNSTOCK CLIP
TUNGSTEN ROD 3/32 in. DIA.
10"
6"
LENSES
16"
24"
QUARTZ TUBE 5/16 in. DIA.
GRADED SEAL

Fig. 5

circuit in turn trips the thyratron which allows the 4 f condenser to discharge through a high tension transformer causing a high frequency spark to traverse the lamps. This spark breaks down the gas within the lamps and allows the large condensers to discharge them. The flash lasts 25 - 50 micro seconds. It has been found convenient to enclose the entire chamber in a dark room and to leave the camera shutter open. A few sample photographs are shown in Fig. 7. The construction of the high tension transformer is illustrated in Fig. 8.

The chamber expansion is tripped by the simultaneous discharge of two Geiger counters. These are so arranged that a particle traversing them must also traverse the central illuminated portion of the chamber. The coincidence circuit, which also acts as a pulse lengthener, is of a conventional design and is shown in Fig.9 for record. The duration of the pulse at different points in the circuit is also indicated. A loud speaker in the plate circuit of the 884 tube indicates whether the counters are functioning properly. The output pulse of this circuit serves to trip the expansion valve, the delay circuit of the flash lamps, the sweep field and the motor controlling a rotary switch (affectionately called the 'sewing machine') which performs a number of switching oper-

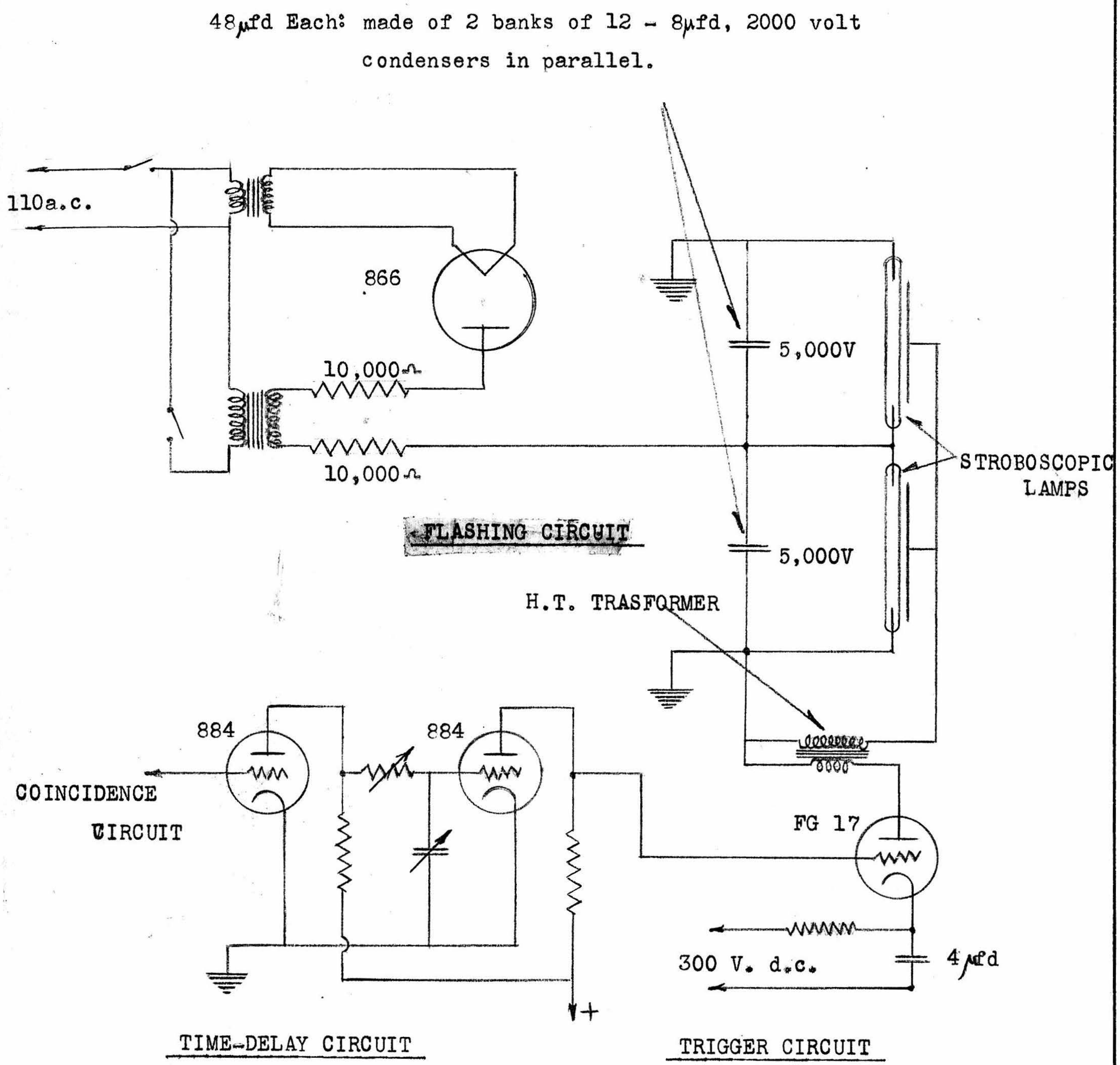

FLASH LAMPS

Fig. 6

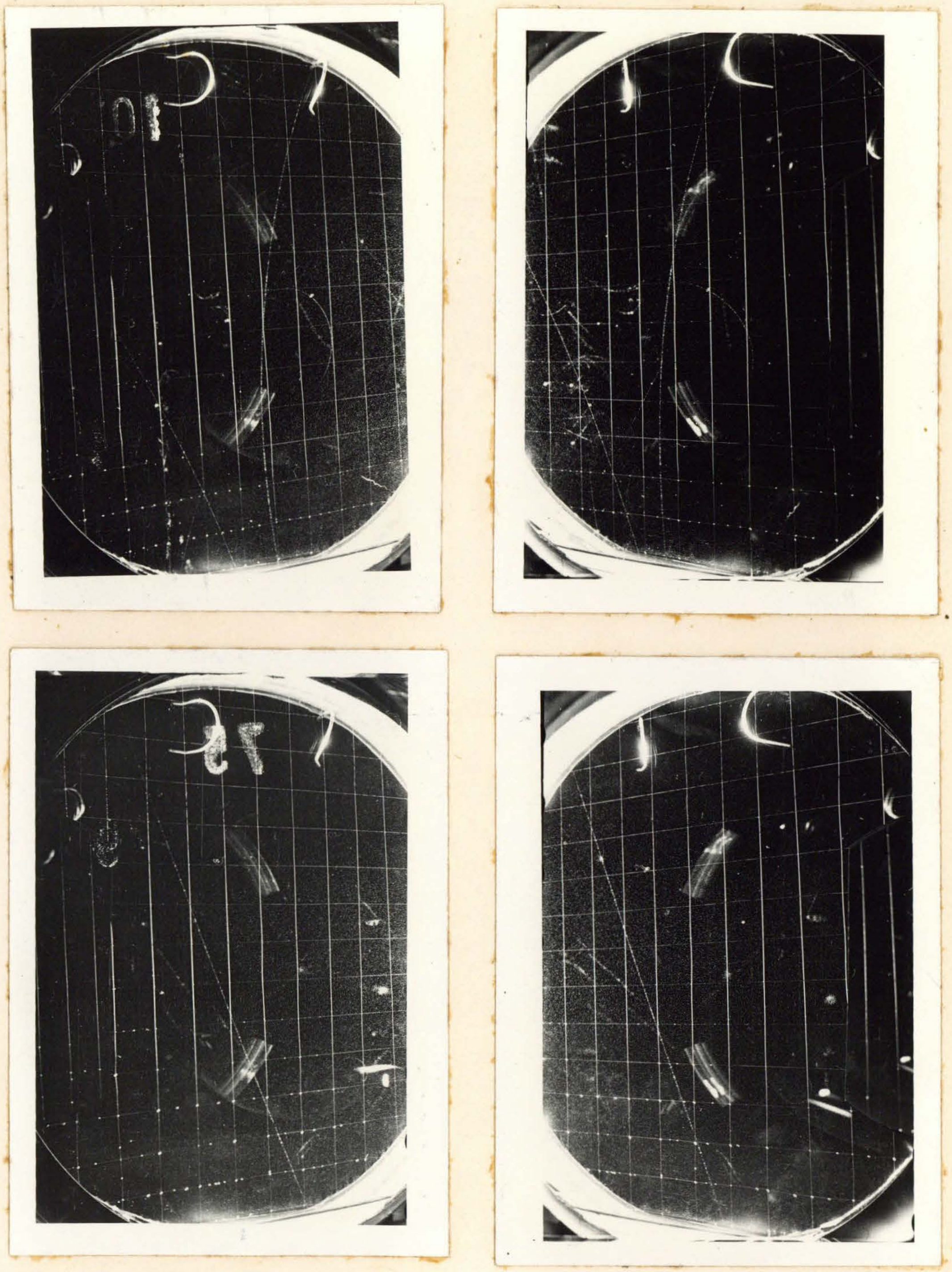

PRINTS OF ACTUAL TRACKS

Fig. 7

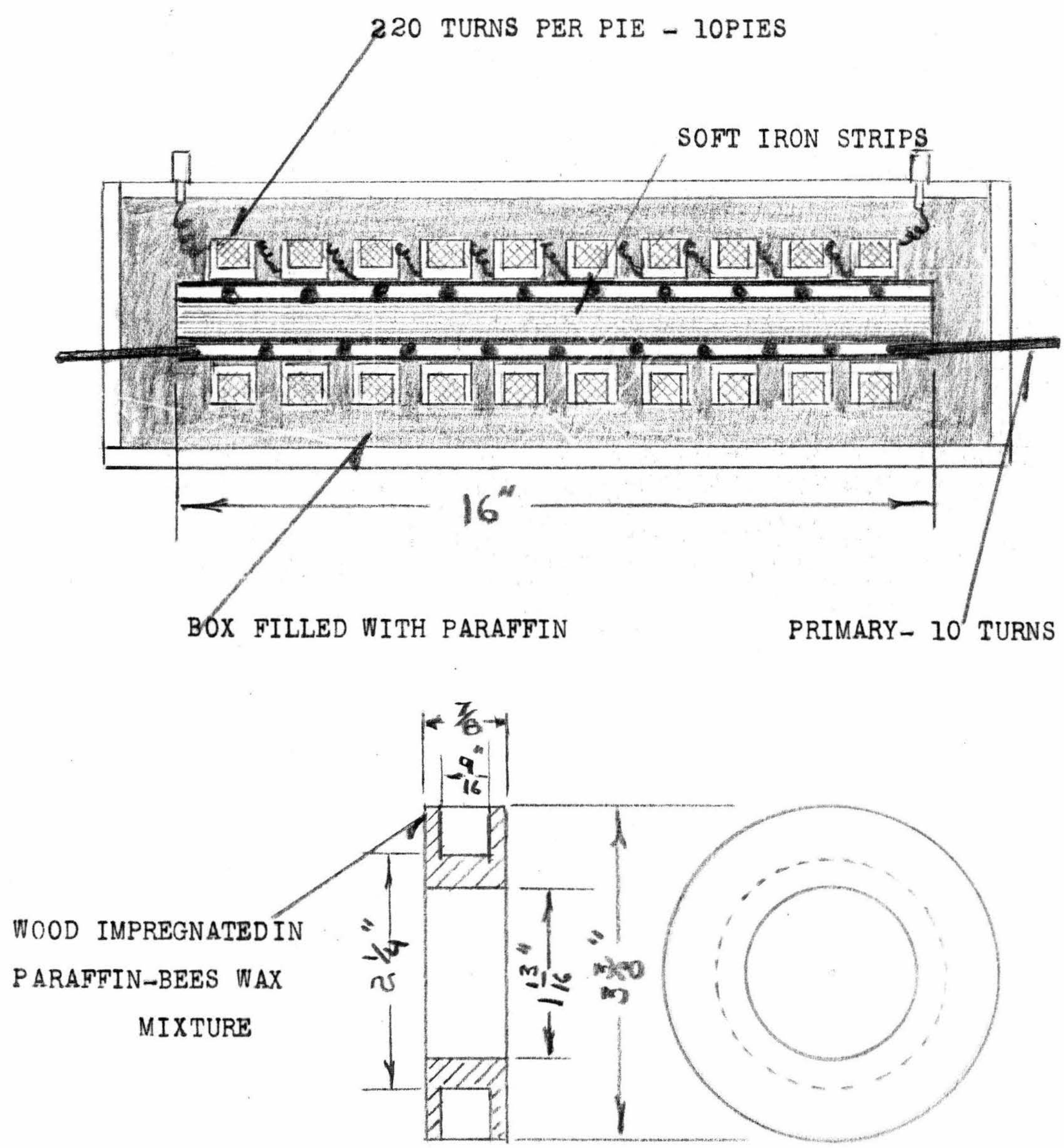

PIE COIL FORM

HIGH TENSION COIL

EACH PIE HAS 11 LAYERS OF 20 TURNS OF NO.28 ENAMEL-COTTON WIRE EACH LAYER WAS COATED WITH HOT PARAFFIN-BEES WAX MIXTURE AND WRAPPED WITH A LAYER OF VARNISH CLOTH.

FIG. 8

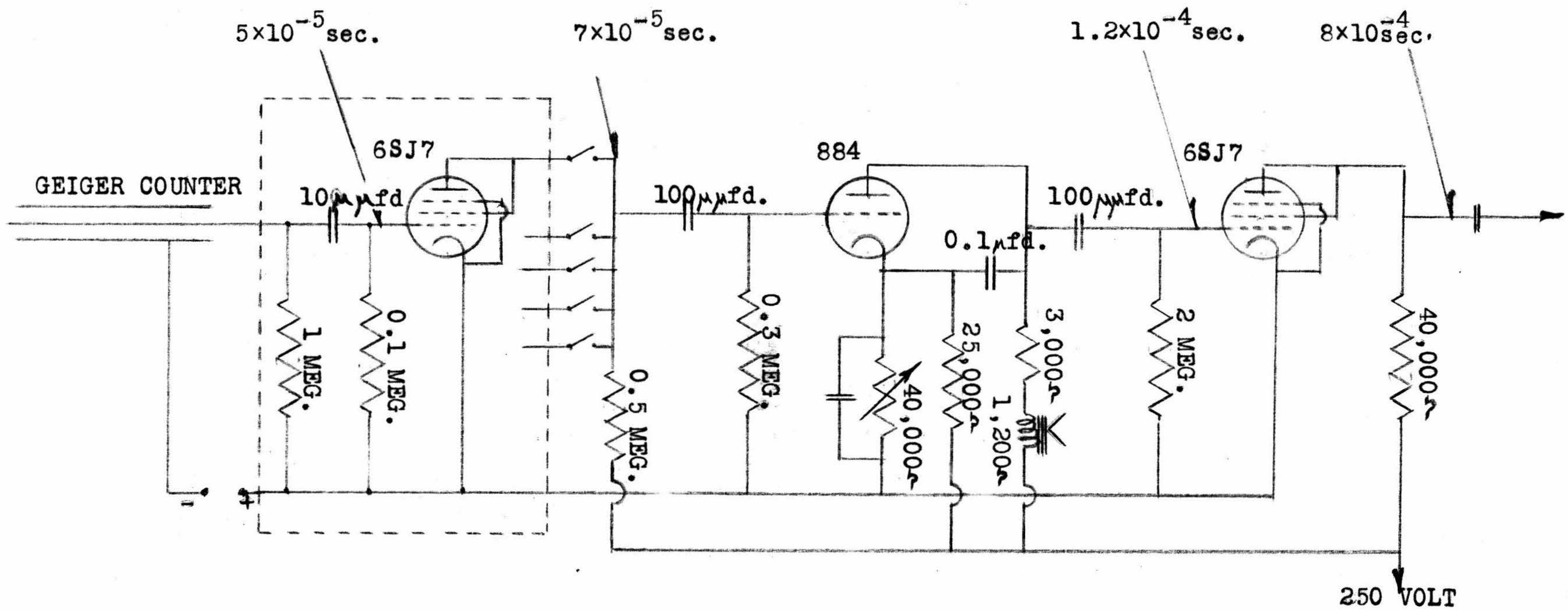

GEIGER COUNTER CIRCUIT

Fig.9

ations in sequence (such as to move the films in the cameras after each exposure, etc.)

The expansion valve is tripped by the firing of an FG17, a relay in series with the plate circuit, serves to interrupt the current allowing the tube to deionize. The inertia of the relay is sufficiently great to allow the expansion valve trip to act.

Considerable trouble was experienced with the sweep circuit. The conventional use of a strip of sheet foil, placed in the cemented joint between the glass ring forming the chamber walls and the front plate of the chamber, to act as one of the electrodes of the sweep field, leads to some difficulties, mainly because the front plate of glass was so large that even when the sweep potential was cut off immediately after the counters were tripped (10^{-3} sec.) the charges accumulated at the center of the plate leaked off slowly and caused seperation of the ions in the track. The difficulty was finally solved by placing an open mesh wire screen (about 2 inches between wires) near the inner front surface of the chamber. Immediately after the chamber expansion this screen was grounded (electronically). Any charges on the glass surface thus had their lines of force terminated on this screen and the chamber was left field free. This mesh is shown in the drawing of Fig. 3 and can be seen as faint squares on the photographs of Fig. 7.

It was found that subjecting the chamber to a slow expansion after each regular expansion reduced the number of background drops considerably, allowing the tracks to stand out more clearly. For this reason a slow expansion valve was incorporated in the chamber mechanism and acted in the sequence of chamber operations.

Summarizing, the sequence of the chamber operations were as follows:

a. Passage of particle through chamber resulted in a coincident discharge of both Geiger counters; the pulse from these passed through the coincidence circuit and was amplified sufficiently to operate the following mechanisms: (i) chamber expansion valve (every effort was made to trip this valve as soon as possible after the passage of the cosmic ray through the chamber); (ii) tripping of lamp flashing circuit; (iii) initiated circuit which dropped potential of sweep screen to zero; (iv) started motor of 'sewing machine' operations will be enumerated as they occurred in time sequence.

b. After an appropriate delay (of the order of .05 sec.) the lamps were flashed and since the cameras had no shutters in them the track was recorded on the film.

c. The 'sewing machine' mechanism got into operation and acted to move the film in the cameras one frame. It also disconnected the tripping mechanism from the Geiger counters so that no further expansions might occurr, until the chamber was again ready. After about fifteen seconds, which was sufficient time to allow the chamber to become compressed, the slow expansion valve was opened for about a minute. At the end of this period of time the valve was closed, the chamber allowed to sit inactive for about a minute, to come to equilibrium, and the counters were again connected leaving everything in readiness for the passage of a new particle.

MEASUREMENT OF TRACKS

As previously mentioned the curvature of the tracks was measured by the aid of the same optical system which had been used to photograph them. The cameras and mirrors were built as a unit on a single frame which could be lifted easily from between the magnet and chamber. This unit is shown in the photograph of Fig. 10. The backs of the cameras were made removable so that projecting lamps could be attached, converting the cameras into projectors. In order to more clearly duplicate the optical path ghrough which the photographs were taken a plate of glass, similar to that forming the front of the cloud chamber, was mounted in front of the cameras and in approximately the same position. The whole unit was placed on a table and a sheet of ground plate glass about three inches wide by three feet long, with a ground glass surface facing the cameras, was placed in front of the unit at approximately the same position where the illuminated portion of the chamber was situated. The track was then projected stereoscopically from the two cameras on this ground surface.

It will be seen that if the ground glass surface is not perfectly plane then a straight line projected on it would appear curved when viewed at an angle to the line of projection. In order to eliminate this source of error and to give a straight line of reference, a fine silk thread was placed

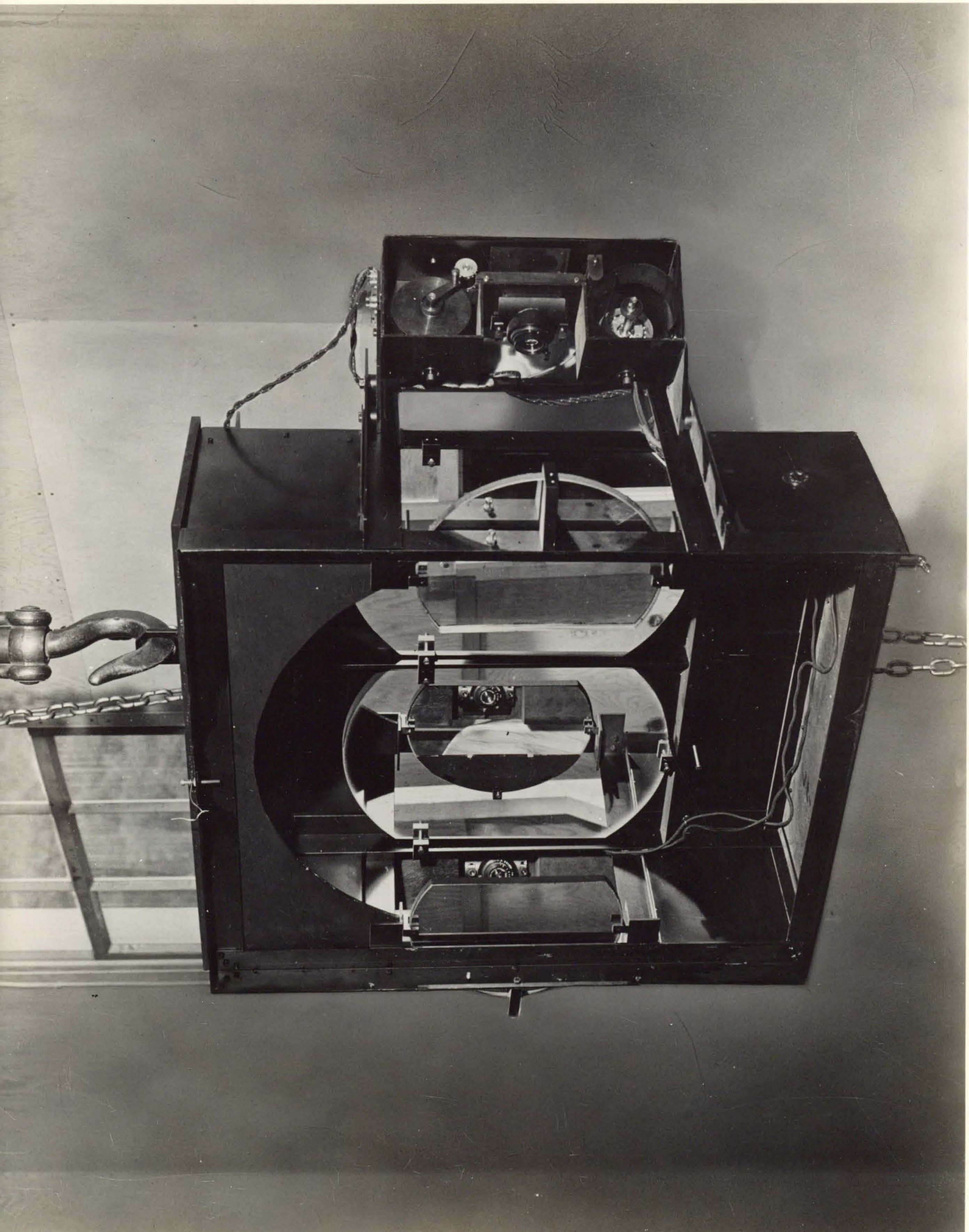

Fig. 22/10

behind the ground glass in such a way that it threw a shadow on the glass. This shadow assumed the same lateral displacement, due to the variations in the plane of the ground glass, as those suffered by the projected track. Thus measurement of the increments between the track and the projected straight line at various points gave the curvature of the track. These measurements were made with a cathetometer eyepiece mounted on a ruled steel support. The support was so mounted that it could be placed parallel to the cosmic ray track under observation. See photograph of Fig. 11. When so arranged the vernier scale in the eyepiece was at right angles to the track whose displacement from the straight line could be measured directly. Readings on the ruled scale of the support located the position of the measured lateral displacement along the track.

MAGNETIC FIELD

The magnetic field between the poles was mapped with the aid of a searching coil. At the center of the chamber, the field strength varied from 4500 gauss at the back of the illuminated portion to 4470 gauss at the front, with 540 amp-

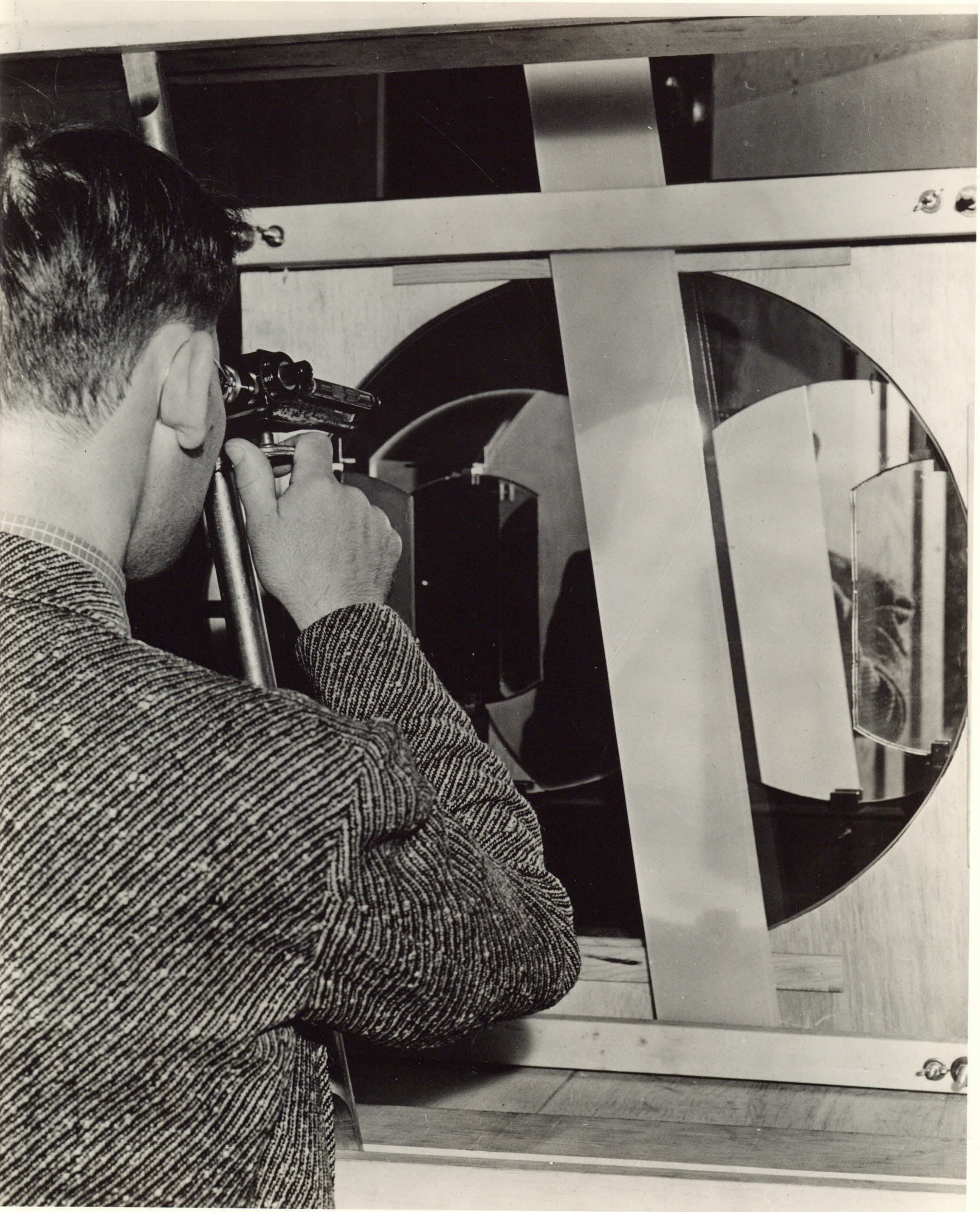

Fig. 11

eres current through the field coils. Curve A of Graph 2.

Further curves are shown on Graph 2. It will be seen that the maximum variation throughout the illuminated portion of the chamber was from 4470 gauss to 5150 gauss, about 14%.

From these measurements the average field over the central plane of the illuminated region was calculated to be 4660 gauss at 540 amperes. Thus the average field at 500 amperes was 4300 gauss, or possibily somewhat higher since the field does not drop off quite as fast as the current.

RESULTS

The results to be reported were taken more in the spirit of working with the chamber and becoming acquainted with its idiosynchrosis in actual use rather than to make any serious study of cosmic rays. It is felt, however, that the data obtained contains sufficient information to make it worth recording.

The chamber was filled with air and saturated with absolute alcohol. As far as could be determined from press-

FIELD STRENGHT AT 540 AMPS.
GRAPH #2

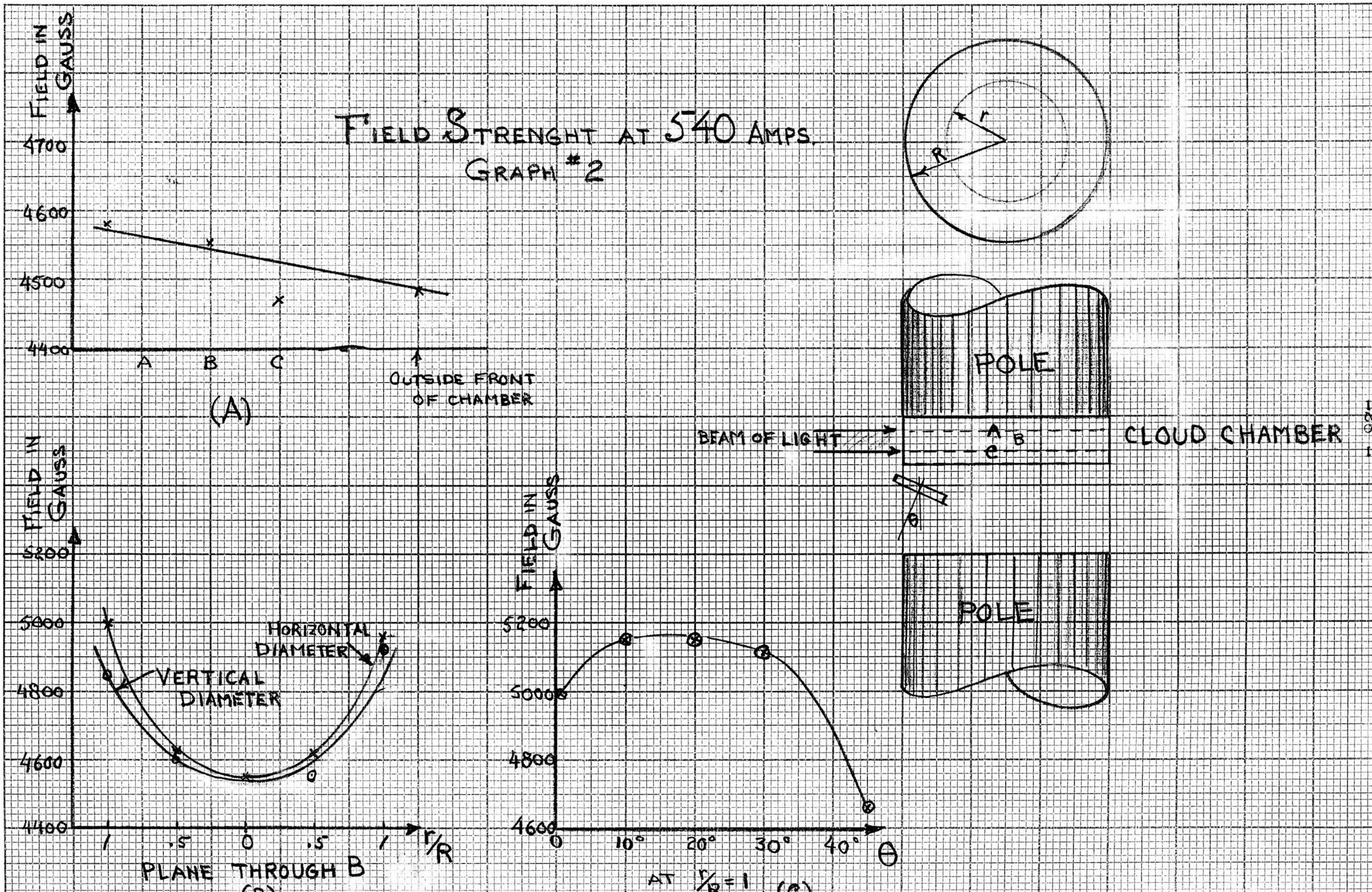

ure measurements the expansion ratio was 1.155, ie. compressed pressure in chamber was 96.2 cm. Hg. while the expanded pressure was 84.2 cm.Hg. at 25.5% (temperature of water from rear water cooled pole); the saturated vapor pressure of ethyl alcohol at this temperature is 6.2 cm.Hg.

Thus

$$\frac{V_2}{V_1} = \frac{96.2 - 6.2}{84.2 - 6.2} = 1.155$$

this seems to be rather low for a chamber filled with air.

On the whole the measurement of track energies in this preliminary test was not too satisfactòry in the higher energy range (over 6 M.E.V.). As far as could be concluded from the limited experience with the chamber the mainsource of error was due to distortions in the tracks themselves and not in the accuracy of curvature measurements. Lateral displacements of individual track points from a straight line could be measured and repeated towithin 0.01 cm. But the resulting curves were not very satisfactory approximations to parabolas in many cases.

Particularly discouraging were some non-field tracks, which showed as high as $1\frac{1}{2}$ mm. first order curvature. It is felt that these are not inherent faults of the apparatus and will be overcome with further work.

The energy of a particle of electronic charge for energies $\gg m_0 C^2$ in terms of the radius of curvatures of its path in magnetic field is given by the well known equation

$$E = 300\ H\rho$$

E = energy of particle in e.v.
ρ = radius of curvature in cm.
H = magnetic field strength in gauss

The radius of curvature may be expressed in terms of the track length and deflection from a straight line by the equation

$$\rho = \frac{h^2}{8\,\delta} \qquad \text{for } \frac{\delta}{h} \ll 1,$$

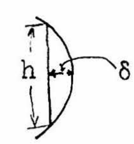

Thus

$$E = \frac{300}{8}\ H\ \frac{h^2}{\delta}$$

Now the average magnetic field at 500 amperes as measured was 4300 gauss, therefore

$$E = 1.61 \times 10^{-4}\ \frac{h^2}{\delta}$$

E in B.E.V.
h and δ in cm.

This is the equation used in the present work to calculate the track energies.

If the error in measuring δ is $\Delta\delta$ $(\delta = \delta_0 \pm \Delta\delta)$ then

$$E = 1.61 \times 10^{-4} \frac{h^2}{\delta_0 \pm \Delta\delta} = 1.61 \times 10^{-4} \frac{h^2}{\delta_0}\left(1 \pm \frac{\Delta\delta}{\delta_0}\right)$$

$$= E_0 \pm \Delta E$$

$$\Delta E = \pm 1.61 \times 10^{-4} \frac{h^2}{\delta_0^2} \Delta\delta \qquad \text{for} \quad \frac{\Delta\delta}{\delta_0} < 1$$

It will also be found convenient to define a curvature σ.

$$\sigma = \frac{10^9}{E} = \frac{6210}{h^2} (\delta_0 \pm \Delta\delta)$$

Assuming $h \approx 50$ cm and $\Delta\delta \approx .02$ cm. Table I gives values of E, σ and ΔE for various values of δ_0

TABLE I

Energy curvature and uncertainty in energy for various values of δ_0 with $h = 50$ cm.

$\Delta\delta = .02$ cm.

$$\Delta\sigma = \pm \frac{6210}{h^2} \Delta\delta = \pm .05$$

δ_0	E	$\pm\ \Delta E$	$\Delta E/E$	σ
0.04 cm	10 BEV	5 BEV	0.5	.099
0.1	4	0.8	0.2	.248
0.2	2	0.2	0.1	.496
0.4	1	0.05	0.05	.992
0.6	0.66	0.022	0.033	1.488
0.8	0.50	0.012	0.024	1.984
1	0.40	0.008	0.02	2.48
2	0.20	0.002	0.01	4.96

A plot of these values is shown in Graph 3.

Altogether 135 tracks were recorded. They are all listed in Table II, showing their energies and signs. To get an idea of the energy spectrum it is necessary to arrange these in groups of definite energy intervals. Unfortunately resulting histogram from such a small number of observations is a function of the size of the energy interval and of the place where its bounderies are chosen. The size of the interval finally chosen ($\frac{1}{2}$ B.E.V.) was sufficiently small not to mask any contour characteristics, yet sufficiently large to constitute a fair statistical group.

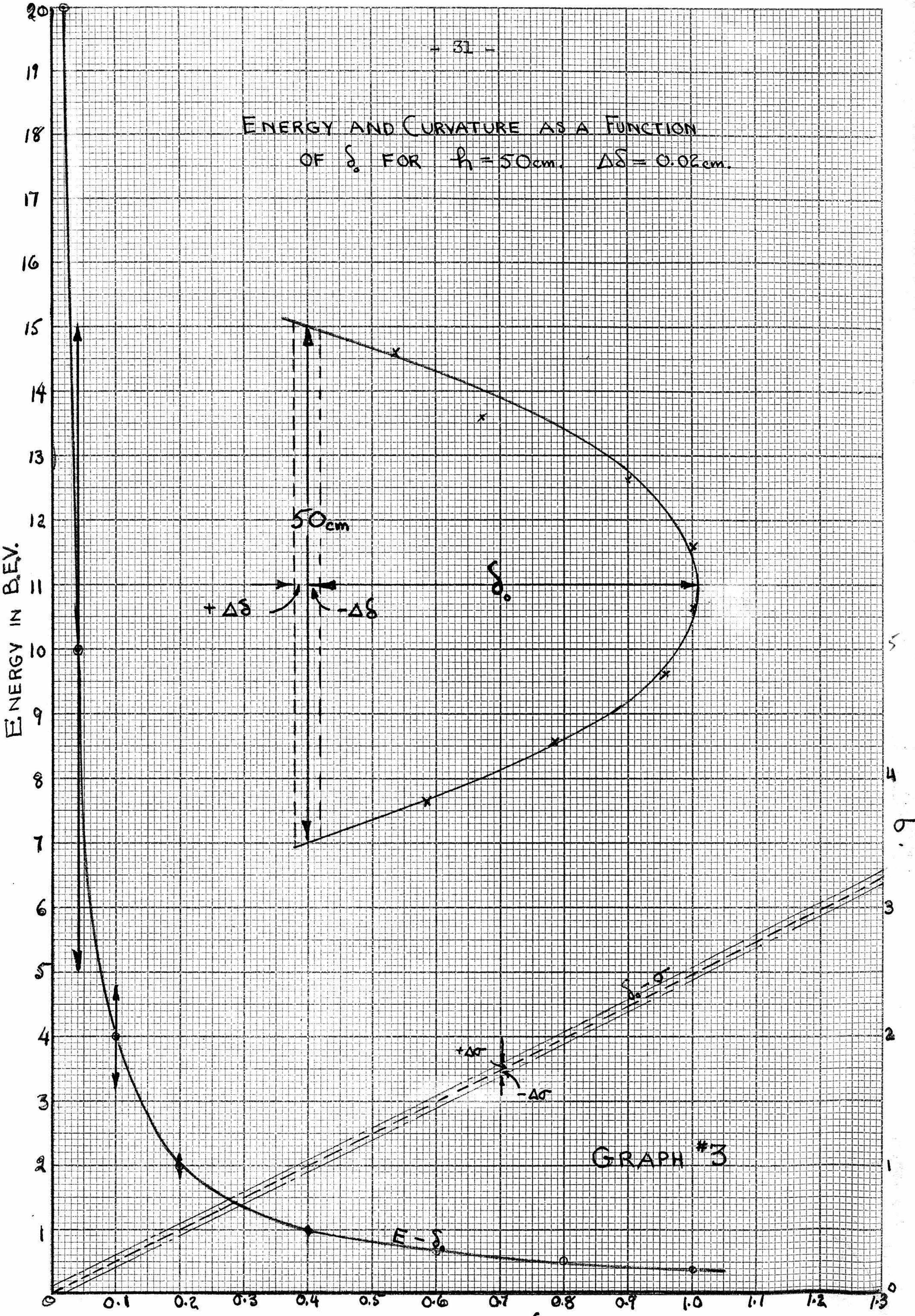
ENERGY AND CURVATURE AS A FUNCTION
OF δ_0 FOR $h = 50$cm. $\Delta\delta = 0.02$cm.
ENERGY IN B.E.V.
δ_0 IN CM.
σ
50cm
δ_0
$+\Delta\delta$
$-\Delta\delta$
$+\Delta\sigma$
$-\Delta\sigma$
$\delta_0 - \sigma$
$E - \delta_0$
GRAPH #3

TABLE III

E	Neg.	Pos.
.08 BEV		1
.10	1	
.12		1
.15	1	
.21		4
.22		1
.24	1	
.26	1	2
.28	1	1
.30	1	
.36		1
.37		1
.38	1	
.39		2
.40	1	
.43	1	1
.45	2	
.48		1
.40	1	
.52		1
.53		1
.54	1	1
.56		1
.58	1	
.62	1	
.65	1	
.66	1	
.67		1
.69	1	
.70	1	1
.71	1	
.73	1	
.82	1	2
.83		1
.84		1
.85	2	
.87		1
.88		1
.89 BEV	1	
.90	1	
.91	1	2
.93		1
.95	1	
.96		2
1.00	1	
1.07	1	
1.10	1	
1.14	1	
1.19		1
1.20	1	
1.29	1	
1.30		1
1.32		1
1.33	1	
1.40		1
1.49	1	2
1.62	1	
1.69		1
1.74		1
1.76		1
1.78		1
1.79		2
1.81		1
1.82	1	
1.83	1	1
1.89	2	1
1.97	1	
2.00		1
2.07	1	
2.20	1	
2.24		1
2.25	1	
2.33	1	
2.44	1	
2.49		2
2.50	2	1
2.60 BEV		1
2.62	1	
2.67	1	
2.69	3	
2.85	1	
3.00	1	
3.10	1	
3.30	1	
3.50		1
3.64	1	
4.57		1
4.60		1
5.10		1
5.18		1
5.80	1	
6.10	1	1
7.44		2
8.80	1	
9.50	1	
10	3	5 (1 doubtful)

To bring out any change in the distribution due to where the interval boundries were chosen the analysis was carried out two ways with the intervals between * 0 - 0.45; 0.46 - 0.95; 0.96 - 1.45 etc. and 0 - 0.20; 0.21 - 0.70; 0.71 - 1.20 etc.

These two types of grouping are shown in Tables III and IV.

TABLE III

Energy Interval	No. Tracks		
	Pos.+ Neg.	Neg.	Pos.
* 0 - .45	28	11	17
0.46 - .95	35	18	17
0.96 - 1.45	13	7	6
1.46 - 1.95	17	6	11
1.96 - 2.45	8	6	2
2.46 - 2.95	12	8	4
2.96 - 3.45	3	3	0
3.36 - 3.95	2	1	1
* 3.96 - 4.95	1	0	1
* 4.96 - 6.95	1.25	0.50	0.75
* 6.96 - 9.45	.60	0.30	0.30
9.45 -	9	3	6

* Table gives number per 1/2 B.E.V. interval

---

* The first interval in each case was corrected by an appropriate weighing factor
ie: 0 - 0.45, number of tracks was multiplied by $\frac{.50}{.45}$

0 - 0.20, number of tracks was multiplied by $\frac{.50}{.20}$

TABLE IV

Energy Interval	No. Tracks		
	Pos.+ Neg.	Neg.	Pos.
* 0 - .20	10	5	5
.21 - .70	37	17	20
.71 - 1.20	27	14	13
1.21 - 1.70	9	4	5
1.71 - 2.20	17	7	10
2.21 - 2.70	15	10	5
2.71 - 3.20	3	3	0
3.21 - 3.70	3	2	1

* Corrected to 1/2 B.E.B. interval

In Table IV the grouping is only carried out to 3.70 B.E.V. which covers the interesting part of the spectrum.

These two sets of data were supperimposed on each other in the form of histograms in graphs 4 (pos. and neg.) 5 (pos.) and 6 (neg.)

Using these curves it was then possible to obtain a set of representative points for drawing distribution curves by taking the mean values of the two sets of data from these graphs. Such average values were taken at 1/4 B.E.V. intervals, as shown by dots on Graph 4, and are plotted in graph No. 7.

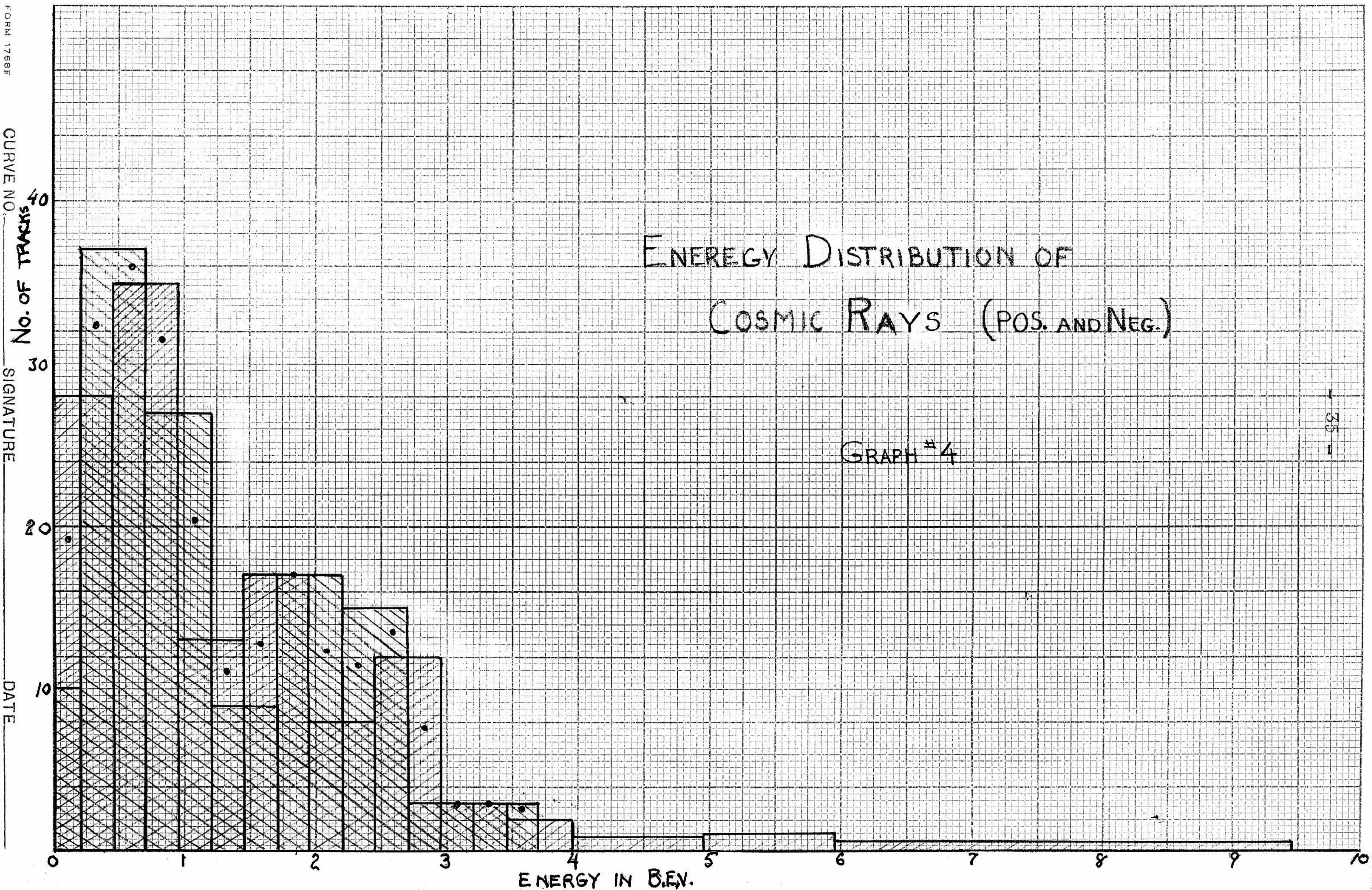
ENEREGY DISTRIBUTION OF
COSMIC RAYS (POS. AND NEG.)
GRAPH #4
No. OF TRACKS
40
30
20
10
0
1
2
3
4
5
6
7
8
9
10
ENERGY IN B.E.V.

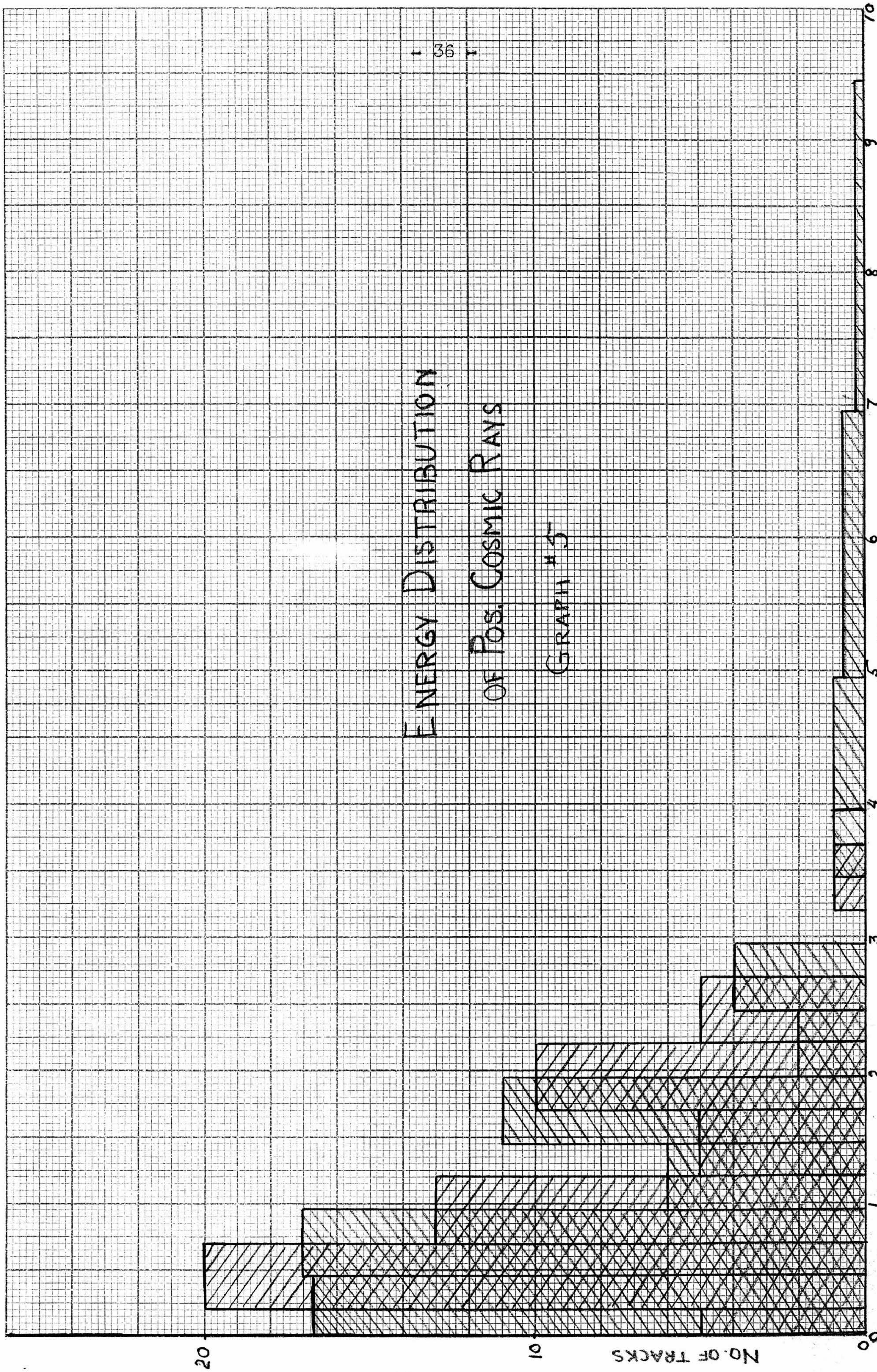
ENERGY DISTRIBUTION
OF POS. COSMIC RAYS
GRAPH #5
ENERGY IN B.E.V.
NO. OF TRACKS
0
1
2
3
4
5
6
7
8
9
10
20

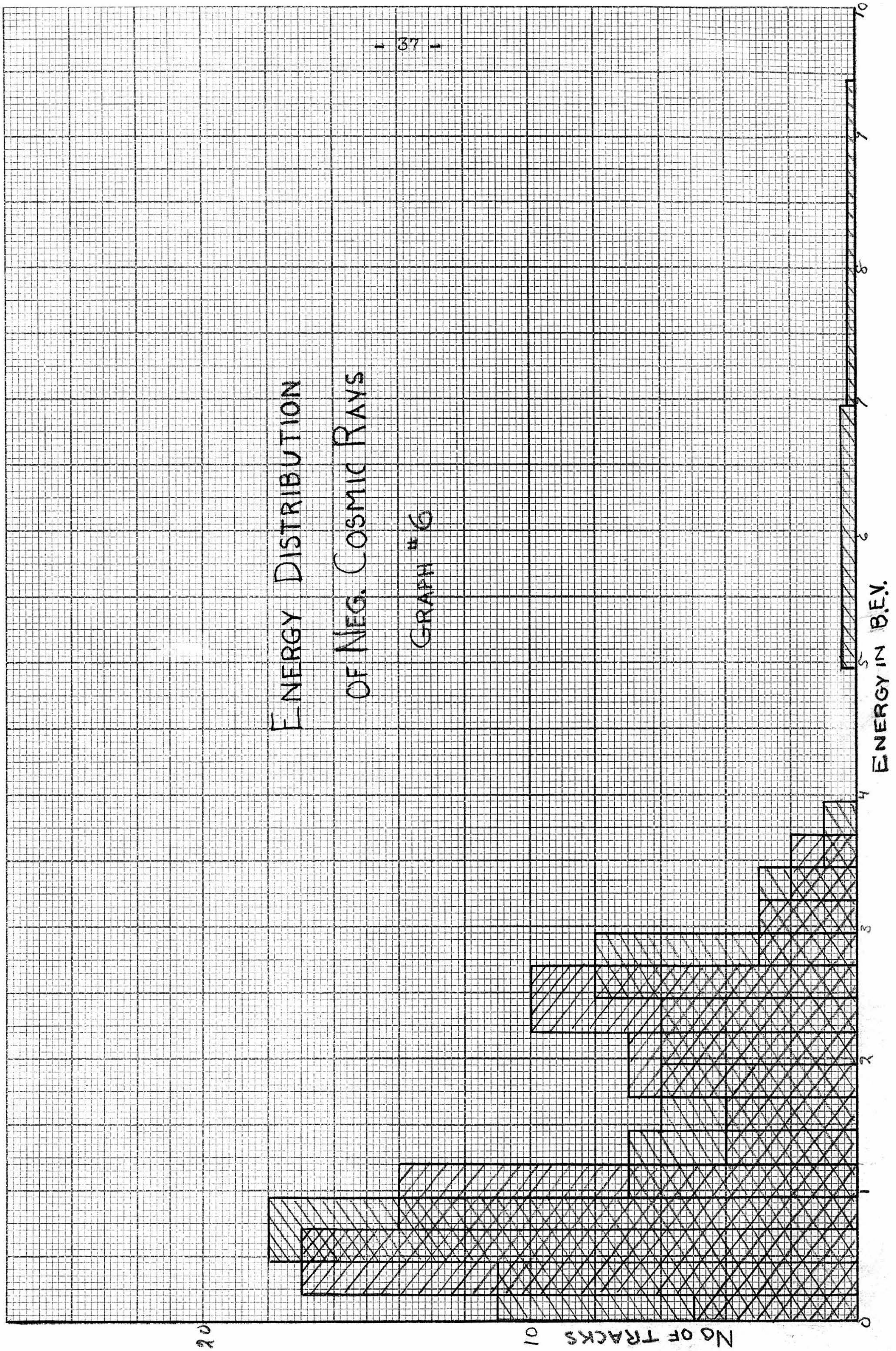
ENERGY DISTRIBUTION
OF NEG. COSMIC RAYS
GRAPH # 6
ENERGY IN B.E.V.
No OF TRACKS
0
1
2
3
4
5
6
7
8
9
10
10
20

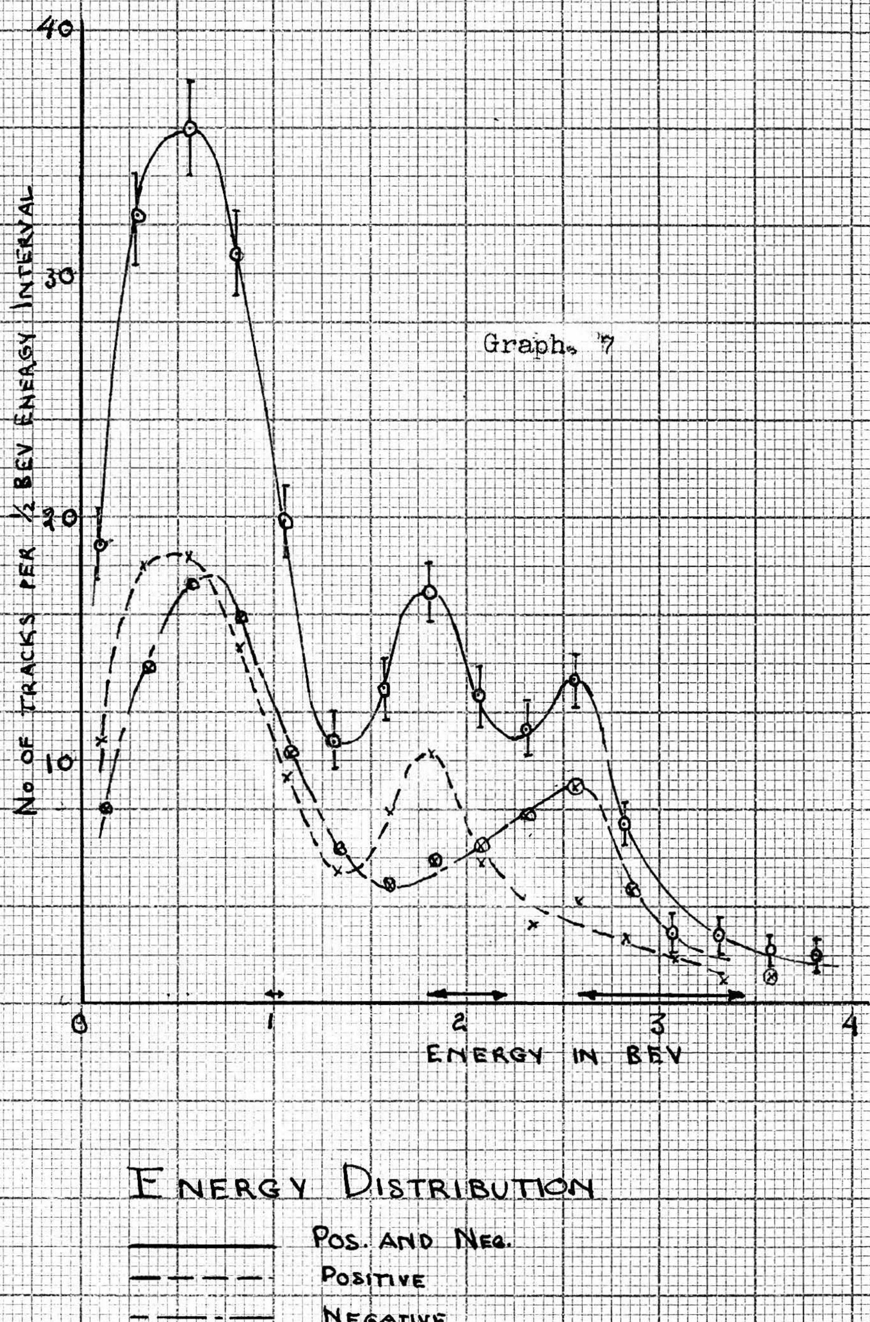

40
30
20
10
0
1
2
3
4
No of tracks per ½ BEV energy interval
Energy in BEV
Graph. 7
Energy Distribution
Pos. and Neg.
Positive
Negative

The curve shows two maxima, one at 1.8 B.E.V. and the other at 2.6 B.E. V. It is seen that one of those maxima is due to the positively charged particles and the other is due to the negatively charged particles.

Careful examination of the energy distribution curve in a paper by Anderson and Neddermyer[1] shows similar secondary maxima. To bring these out more clearly the data given in that paper was analysed by the method of overlapping histograms (of 1/2 BEV intervals) and the resulting curve is shown in Graph 8. This graph also displays two maxima, though at somewhat higher energies. A similar analysis was carried out on data published by Blackett[2] and the distribution obtained is shown in Graph 9. Blackett's data shows one maxima, however Blackett points out that Fig. 7 of his paper shows two minima, one at $E \approx 2.2$ BEV, the other at $E \approx 1.25$ BEV. The one at 2.2 BEV is taken to be experimentally established and the other at 1.25 BEV to be 'probably real'. The two minima in our graphs are surprisingly close to these values. The reason why the minima at 1.25 BEV does not appear on Graph 9 of this paper seems to be because of its extreme narrowness, being of the order of 0.2 BEV.

---

[1] Fundamental Processes in the Absorption of Cosmic Ray Electrons and Photons - C. D. Anderson and S.H. Neddermeyer - Papers and Discussions of the International Conference on Physics, London, 1934, Nuclear Physics.

[2] Further Measurements of the Cosmic Ray Energy Spectrum - P.M.S. Blackett, Proc. Roy. Soc. Lon. 159, 1 (1937)

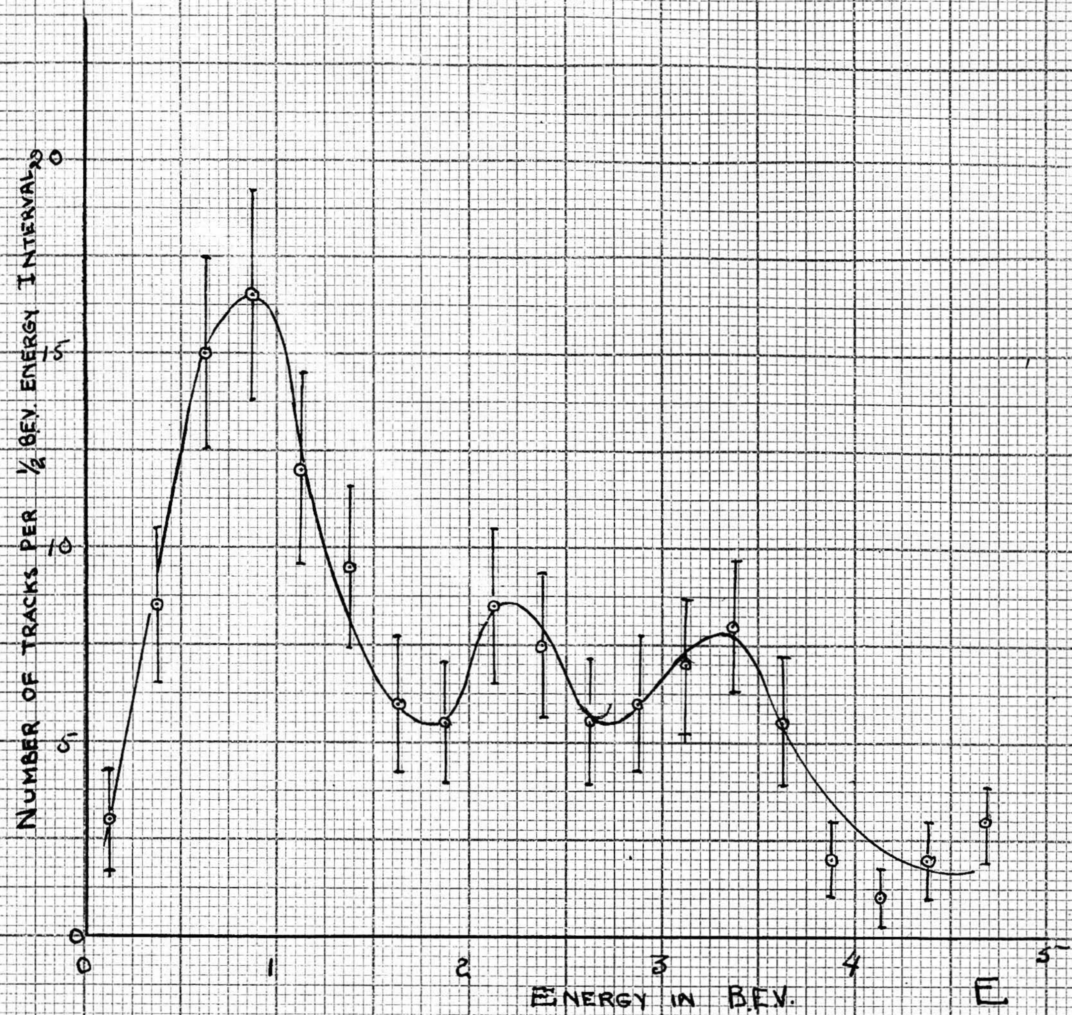

ENERGY DISTRIBUTION
OF
POSITIVE AND NEGATIVE PARTICLES OCCURING SINGLY

ACCORDING TO ANDERSON AND NEDDERMEYER

Graph 9

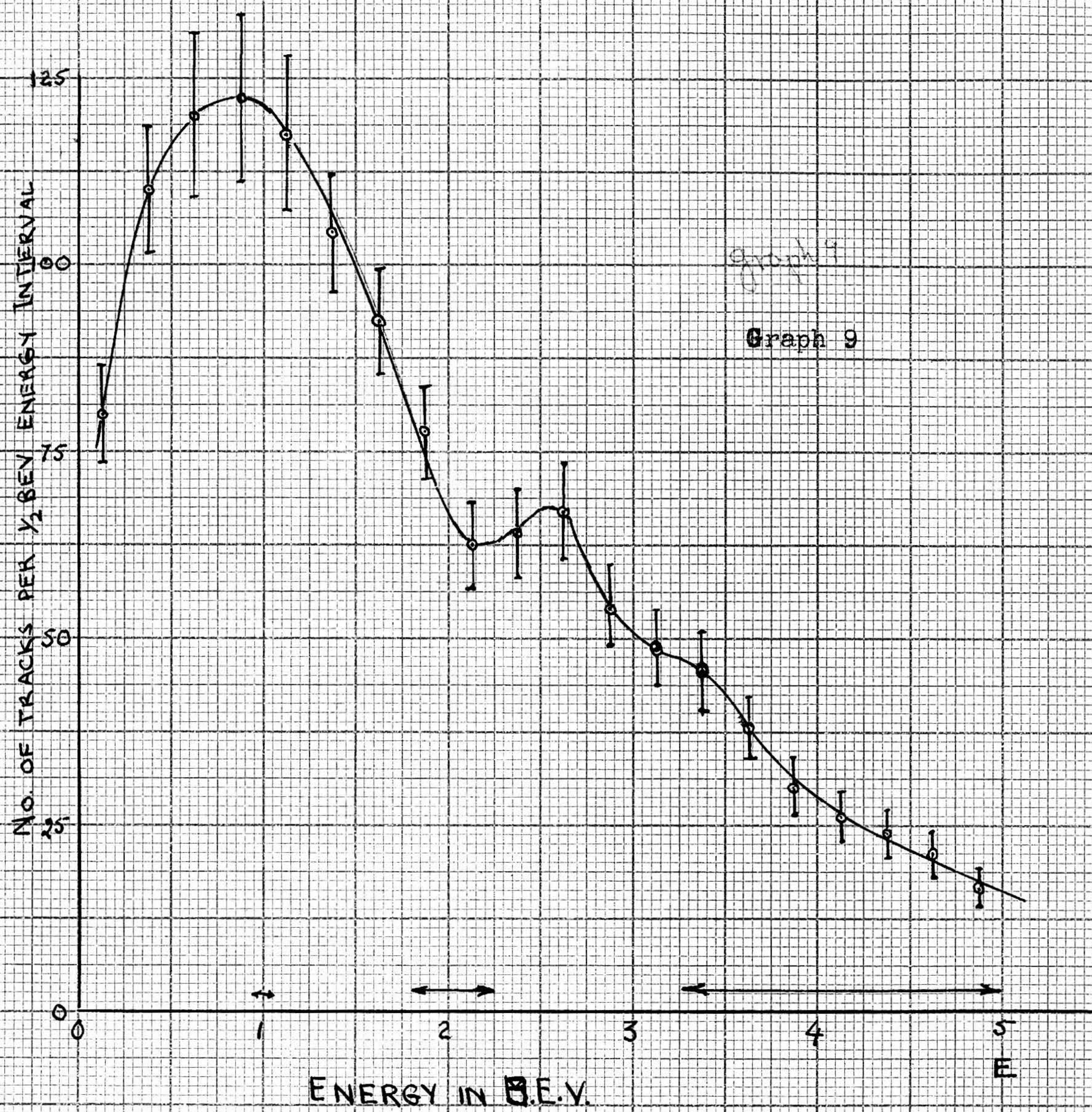

ENERGY DISTRIBUTION
OF
POSITIVE AND NEGATIVE TRACKS

ACCORDING TO BLACKETT

FORM 1768E CURVE NO.__________ SIGNATURE__________ DATE__________

The vertical lines drawn through the experimental points of each graph give the probable error according to $\Delta N = \pm .68 \sqrt{N}$, and the horizontal double headed arrows give ΔE at the various energies; those in Graph 7 are according to Table I, whereas those in Graph 9 were taken from Blackett's paper.

Since in the energy distribution graphs ΔE varies as E^2 it would be more instructive to examine the $N - \sigma$ curves in which $\Delta\sigma$ is a constant independent of σ.

The energies of Table II were expressed in terms of σ and the resulting distribution was then divided in two manners into groups of $\sigma = 0.2$ wide. These groups had boundries at 0 - .2, .2 - .3, .4 - .6, etc. and 0 -.1, .1 -.3, .3- .5. As before the overlapping hestograms were drawn and average values were taken from these distributions shown in Graph 10 were obtained. The distribution curve of the N_{p+N} tracks shows two maxima, the one at $\sigma = 1.2$ corresponds to the first large maxima at E .8 BEV, the other at $\sigma = .45$ corresponds to the two secondary maxima, here the two peaks are crowded so closely together ($\sigma = .15$ apart) that they are not resolved.

Blackett has suggested that the secondary maxima may be due to selective absorption of the rays as they pass through

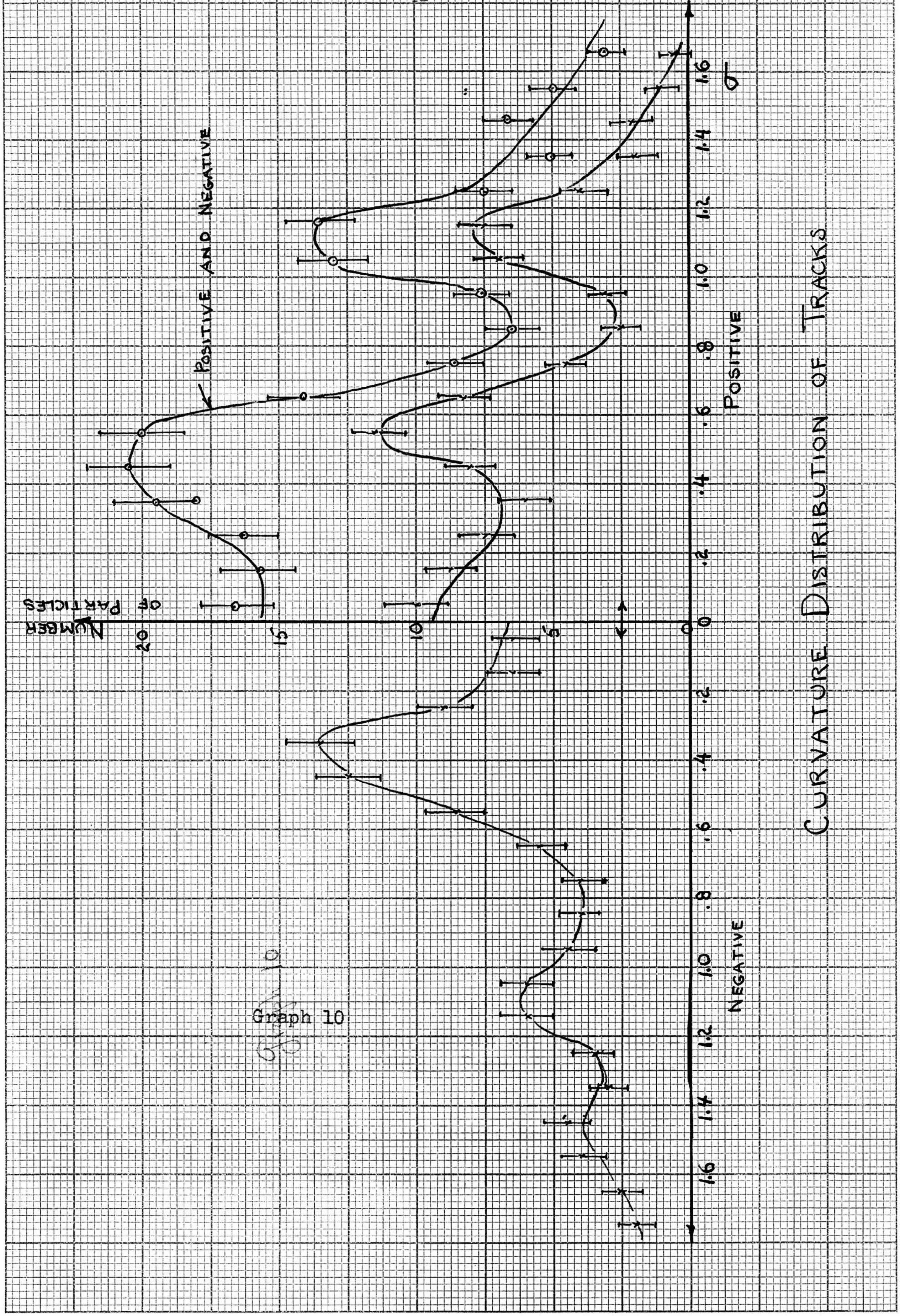

Graph 10

FORM 1768E CURVE NO.__________ SIGNATURE__________ DATE__________ the atmosphere . As an alternative cause, it is interesting to speculate that the observed energy spectrum is due to a structure in the primaries. One might even venture to tie it up with the banded structure proposed by Millikan and Neher.[3]

---

3 Energy Distribution of Incoming Cosmic Ray Particles - R. A. Millikan and H.V. Neher, Proc. Am. Acd. Sci. 83, 409, (1940)

A Hypothesis as to the Origin of Cosmic Rays and the Experimental Testing in India and Elsewhere - Millikan, Neher and Pickering, Phys. Rev. 61, 397, (1942)